Large eddy simulation of turbulent channel flows by the rational large eddy simulation model

Traian Iliescu and Paul F. Fischer

Citation: Physics of Fluids (1994-present) **15**, 3036 (2003); doi: 10.1063/1.1604781
View online: http://dx.doi.org/10.1063/1.1604781
View Table of Contents: http://scitation.aip.org/content/aip/journal/pof2/15/10?ver=pdfcov
Published by the AIP Publishing

Large eddy simulation of turbulent channel flows by the rational large eddy simulation model

Traian Iliescu
Department of Mathematics, Virginia Polytechnic Institute and State University, Blacksburg, Virginia 24061

Paul F. Fischer
Mathematics and Computer Science Division, Argonne National Laboratory, Argonne, Illinois 60439

(Received 20 March 2003; accepted 8 July 2003; published 4 September 2003)

The rational large eddy simulation (RLES) model is applied to turbulent channel flows. This approximate deconvolution model is based on a rational (subdiagonal Padé) approximation of the Fourier transform of the Gaussian filter and is proposed as an alternative to the gradient (also known as the nonlinear or tensor-diffusivity) model. We used a spectral element code to perform large eddy simulations of incompressible channel flows at Reynolds numbers based on the friction velocity and the channel half-width $\mathrm{Re}_\tau=180$ and $\mathrm{Re}_\tau=395$. We compared the RLES model with the gradient model and the Smagorinsky model with Van Driest damping. The RLES model was much more stable than the gradient model and yielded improved results. Both the RLES model and the gradient model predicted the off-diagonal Reynolds stresses better than the Smagorinsky model with Van Driest damping. The latter, however, yielded better results for the diagonal Reynolds stresses. © *2003 American Institute of Physics.* [DOI: 10.1063/1.1604781]

I. INTRODUCTION

Large eddy simulation (LES) is one of the most successful techniques in the numerical simulation of turbulent flows. Contrary to the direct numerical simulation (DNS), which tries to capture all the scales in the flow, LES aims at resolving only the large-scale flow features. The large scales are defined by means of a filtering operation: the Navier–Stokes equations are convolved with a spatial filter, and the resulting filtered variables become the variables of interest in LES. Thus, a good LES model should be able to compute an accurate approximation of the filtered variables.

An essential challenge in LES is the modeling of the subfilter-scale (SFS) stresses, representing the interactions between the large (above the filter width) and small (below the filter width) scales in the filtered Navier–Stokes equations. A remarkable research effort has led to a wide variety of SFS models, surveyed, for example, in Refs. 1–3.

Arguably the most popular class of LES models is the eddy-viscosity type, based on (variants of) the Smagorinsky model.[4] The main feature of the eddy-viscosity models is that they properly transfer kinetic energy (by inviscid processes) from large scales to smaller and smaller scales, until this energy is dissipated through viscous effects. These models have several limitations, however, including poor correlation coefficients in *a priori* tests[5,6] and inability to provide backscatter. Some of these limitations are circumvented by using a dynamic procedure in calculating the Smagorinsky constant, yielding the dynamic subgrid-scale eddy-viscosity model introduced by Germano *et al.*,[7] and used in many studies.[8,9]

Another class of LES models is the scale-similarity one. The scale-similarity model, introduced by Bardina *et al.*,[6] postulates that the full structure of the velocity field at scales below the filter width is similar to that at scales above the filter width. *A priori* tests[6] show high correlations between real and modeled stresses. Another realistic feature of the scale-similarity model is that it produces backscatter. In *a posteriori* tests, however, the scale-similarity model does not dissipate enough energy and typically leads to inaccurate results. As a remedy, Bardina *et al.*[6] added a dissipative Smagorinsky term. The resulting model, known as the mixed model, combines the strengths of both the scale-similarity and the Smagorinsky model. The dynamic procedure has been successfully applied to both the pure and the mixed scale-similarity model, yielding improved results.[10]

A different class of LES models consists of those models aimed at computing an improved SFS stress approximation by replacing the unknown unfiltered variables with approximately deconvolved filtered variables. An inverse filtered model was first proposed by Shah and Ferziger.[11] This idea was formalized by Geurts[12] for the top hat filter. Kuerten *et al.*[13] used the approximate inverse to improve the computable estimates in the dynamic Smagorinsky model. Another model in this class is the velocity estimation model of Domaradzki and Saiki.[14–16] Stolz and Adams[17] developed the approximate deconvolution model, based on repeated application of the filter to approximately deconvolve the dependent variables.[18,19]

One popular model in this class is the gradient model (also known as the nonlinear or tensor-diffusivity model), which uses *explicit* filtering. In addition to the *implicit* filtering due to the effective truncations (grid and numerical method), this LES model also assumes a regular explicit filter of prescribed shape and effective width larger than the grid spacing.

The gradient model is based on a Taylor series approximation of the Fourier transform of the filter and aims at reconstructing the filtered-scale stress due to explicit filter-

ing. The gradient model was developed in several steps. First, in 1974 Leonard[20] proposed a model for the ''resolved scales'' $\overline{\mathbf{u}}\overline{\mathbf{u}}$ in the Reynolds stress tensor. Next, in 1979, Clark, Ferziger, and Reynolds[5] used the same approach to model the ''cross terms'' $\overline{\mathbf{u}}\mathbf{u}'+\mathbf{u}'\overline{\mathbf{u}}$.

The gradient model was tested *a priori* against experimental data (two-dimensional cuts) by Liu *et al.*[21] Borue and Orszag[22] presented a detailed *a priori* analysis of the gradient model based on Gaussian-filtered DNS of homogeneous, isotropic decaying turbulence. Also, Winckelmans *et al.*[23] presented several *a priori* tests for the gradient model and its dynamic version, again in the context of homogeneous, isotropic decaying turbulence. Similar tests have been performed by Carati *et al.*[24] All the above *a priori* tests have shown high correlations.

In *a posteriori* tests, however, it was found that the gradient model does not dissipate enough energy. Simulations with the pure gradient model appear to be unstable.[25] Also, Liu, Meneveau, and Katz[21] reported problems near the wall, where the pure gradient model's Reynolds stresses do not follow the x_2^3 behavior. To stabilize the gradient model, Clark, Ferziger, and Reynolds[5] combined it with a Smagorinsky term, but the resulting mixed model inherited the excessive dissipation of the Smagorinsky model. A different approach was proposed by Liu *et al.*,[21] who supplied the gradient model with a ''limiter'' to prevent energy backscatter; this clipping procedure ensures that the model dissipates energy from large to small scales. This approach was also used in Refs. 26, 27.

From this point of view, the gradient model is similar to the scale-similarity model: It shows high correlations in *a priori* tests, but it does not dissipate enough energy in actual LES simulations: hence, the need for extra viscosity type terms (mixed models). We note that, for both types of model, the best results in actual LES simulations were obtained by using the dynamic mixed procedure.[23,28] In fact, it has been noted before[9,23,24,28] that there are strong ties between the gradient model and the scale-similarity model: the first term in the Taylor series expansion of the scale-similarity model is indeed the gradient model. As noted by Winckelmans *et al.*,[23] however, the other terms in the expansion are different. Thus, the gradient model is not identical to the scale-similarity model.

The model presented in this paper was introduced by Galdi and Layton[29] as an alternative to the gradient model. They observed that the Taylor series approximation of the Fourier transform of the Gaussian filter used in the derivation of the gradient model actually *increases* the high wave number components, instead of damping them. As an alternative to the Taylor series approximation, Galdi and Layton proposed a rational [(0,1) Padé)] approximation. This rational approximation is consistent with the original approximated function (which is a negative exponential): it attenuates the high wave number components.

In this paper, the resulting LES model, called in the sequel the rational LES (RLES) model, is applied to the numerical simulations of incompressible channel flows at $\mathrm{Re}_\tau=180$ and $\mathrm{Re}_\tau=395$.

II. THE RATIONAL LES MODEL

The usual LES starts by convolving the Navier–Stokes equations (NSEs) with a spatial filter g_δ. Assuming that differentiation and convolution commute (which is true for homogeneous filters), the filtered NSEs read as follows:

$$\overline{\mathbf{u}}_t+\nabla\cdot(\overline{\mathbf{u}\mathbf{u}})-\mathrm{Re}^{-1}\Delta\overline{\mathbf{u}}+\nabla\overline{p}=\overline{\mathbf{f}}, \tag{1}$$

where δ is the filter width and $\overline{\mathbf{u}}=g_\delta*\mathbf{u}$ is the variable of interest. The filtered NSEs (1) do not form a closed system, and a considerable research effort in LES research has been directed at modeling the stress

$$\tau=\overline{\mathbf{u}\mathbf{u}}-\overline{\mathbf{u}}\overline{\mathbf{u}}. \tag{2}$$

As mentioned by Carati *et al.*,[24] this stress consists of a subfilter-scale stress tensor, mainly due to filtering, and a subgrid-scale (SGS) stress tensor, mainly due to discretization. One way of approximating the subfilter-scale stress tensor is by using a Taylor series expansion in the wave number space to represent the unknown full velocity in terms of the filtered velocity. This approach was first used by Leonard,[20] and it was later espoused by Clark, Ferziger, and Reynolds.[5] The resulting model, called the gradient, nonlinear, or tensor-diffusivity model, was used in numerous studies.[5,20–24,30–32]

The gradient model is derived by using a Taylor series approximation to the Fourier transform of the Gaussian filter

$$\widehat{g_\delta}(\mathbf{k})=e^{-\delta^2|\mathbf{k}|^2/4\gamma}\approx 1-\frac{\delta^2|\mathbf{k}|^2}{4\gamma}+O(\delta^4), \tag{3}$$

and for its inverse

$$\frac{1}{\widehat{g_\delta}(\mathbf{k})}=e^{\delta^2|\mathbf{k}|^2/4\gamma}\approx 1+\frac{\delta^2|\mathbf{k}|^2}{4\gamma}+O(\delta^4). \tag{4}$$

Decomposing $\mathbf{u}$ into its average and its turbulent fluctuations

$$\mathbf{u}=\overline{\mathbf{u}}+\mathbf{u}', \tag{5}$$

and taking first the average and then the Fourier transform of the above relation, we get

$$\hat{\mathbf{u}}'=\left(\frac{1}{\widehat{g_\delta}}-1\right)\hat{\overline{\mathbf{u}}}, \tag{6}$$

and thus

$$\hat{\mathbf{u}}=\frac{1}{\widehat{g_\delta}}\hat{\overline{\mathbf{u}}}, \tag{7}$$

where $\hat{\mathbf{u}}$ denotes the Fourier transform of $\mathbf{u}$.

By taking the inverse Fourier transform and using (4), we get

$$\mathbf{u}\approx\overline{\mathbf{u}}-\frac{\delta^2}{4\gamma}\Delta\overline{\mathbf{u}}. \tag{8}$$

By plugging the above into (2), using (3) and the same technique as above, simplifying, and dropping out the terms of $O(\delta^4)$, we get the gradient model

$$\tau=\overline{\mathbf{u}\mathbf{u}}-\overline{\mathbf{u}}\overline{\mathbf{u}}\approx\frac{\delta^2}{2\gamma}\nabla\overline{\mathbf{u}}\nabla\overline{\mathbf{u}}, \tag{9}$$

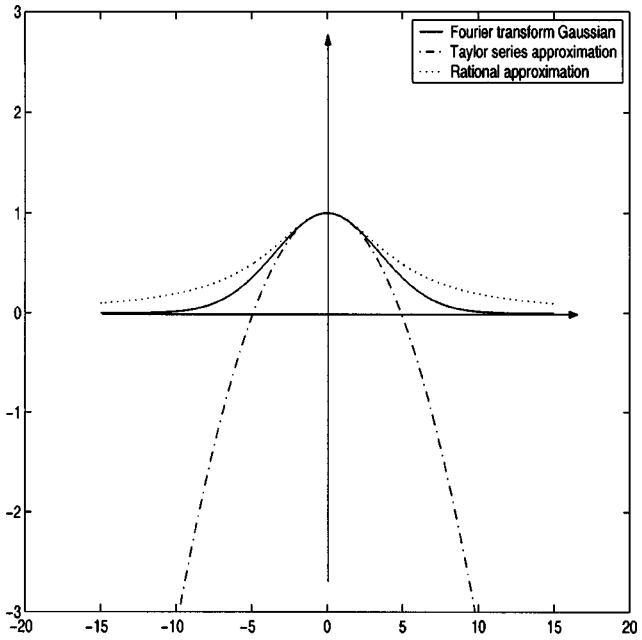

FIG. 1. Approximations to the Fourier transform of the Gaussian filter: Rational (Padé) vs Taylor.

where

$$(\nabla\overline{\mathbf{u}}\nabla\overline{\mathbf{u}})_{i,j}=\sum_{l=1}^{d}\frac{\partial\overline{\mathbf{u}}_i}{\partial\mathbf{x}_l}\frac{\partial\overline{\mathbf{u}}_j}{\partial\mathbf{x}_l}. \tag{10}$$

Noticing that the approximation by Taylor series of $\widehat{g_\delta}$ actually *increases* the high wave number components (see Fig. 1), Galdi and Layton[29] developed a new LES model based on a rational [(0,1) Padé] approximation of $\widehat{g_\delta}$, which preserves the decay of the high wave number components

$$\widehat{g_\delta}(\mathbf{k})=e^{-\delta^2|\mathbf{k}|^{2'}/4\gamma}\approx\frac{1}{1+\dfrac{\delta^2|\mathbf{k}|^2}{4\gamma}}+O(\delta^4). \tag{11}$$

The resulting LES model, called the rational LES (RLES) model, reads as follows:

$$\tau=\left[\left(-\frac{\delta^2}{4\gamma}\Delta+I\right)^{-1}\left(\frac{\delta^2}{2\gamma}\nabla\overline{\mathbf{u}}\nabla\overline{\mathbf{u}}\right)\right]. \tag{12}$$

The inverse operator in (12) acts as a smoothing operator and represents the approximation of the convolution by the Gaussian filter in the stress tensor τ in (2).

We note that differential filters have been proposed by Germano in Ref. 33: Actually, one can think of (12) as the stress tensor obtained by applying such a differential filter. Mullen and Fischer used similar filters in Ref. 34. Also, Domaradzki and Holm considered the Navier–Stokes-alpha model [which contains an inverse operator similar to the one in (12)], in an LES framework.[35]

The mathematical analysis associated with the RLES model (12) was presented in Ref. 36. The first steps in the numerical analysis and validation of the RLES model (12) were made in Refs. 37 and 38, respectively.

This paper presents numerical results for the RLES model (12) applied to the 3D channel flow test problem at

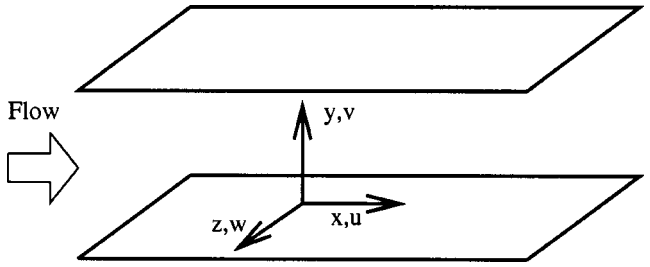

FIG. 2. Problem setup for the channel flow.

Reynolds numbers based on the wall shear velocity $\mathrm{Re}_\tau=180$ and $\mathrm{Re}_\tau=395$. Some preliminary work started in Ref. 39; it was significantly updated and improved in the present paper.

III. NUMERICAL SETTING

The 3D channel flow (Fig. 2) is one of the most popular test problems for the investigation of wall bounded turbulent flows.[40,41] We used the fine DNS of Moser, Kim, and Mansour[42] as benchmark for our LES simulations.

We compared the RLES model (12) with

(I) the gradient model (9) $\tau=(\delta^2/2\gamma)\nabla\overline{\mathbf{u}}\nabla\overline{\mathbf{u}}$;
(II) the Smagorinsky model with Van Driest damping $\tau=-(C_s\delta(1-\exp(-y^+/A^+))^2|\overline{S}|\overline{S}$, where $\overline{S}:=\frac{1}{2}(\nabla\overline{\mathbf{u}}+\nabla\overline{\mathbf{u}}^T)$ is the deformation tensor of the filtered field, $C_s=0.1$ is the Smagorinsky constant, $\gamma=6$ is the parameter in the definition of the Gaussian filter, $y^+=(H-|y|)u_\tau/\nu$ is the nondimensional distance from the wall, $H=1$ is the channel half-width, u_τ is the wall shear velocity, and $A^+=25$ is the Van Driest constant.

The computational domain is periodic in the streamwise (x) and spanwise (z) directions, and the pressure gradient that drives the flow is adjusted dynamically to maintain a constant mass flux through the channel. The parameters used in the numerical simulations are given in Table I for the two Reynolds numbers considered ($\mathrm{Re}_\tau=180$ and $\mathrm{Re}_\tau=395$).

The filter width δ is computed as $\delta=\sqrt[3]{\Delta_x\Delta_z\Delta_y(y)}$, where Δ_x and Δ_z are the largest spaces between the Gauss–Lobatto–Legendre (GLL) points in the x and z directions, respectively, and $\Delta_y(y)$ is inhomogeneous and is computed as an interpolation function that is zero at the wall and is twice the normal mesh size for the elements in the center of the channel. Note that, since we filter in all three directions, the filter width δ never vanishes away from the wall. This, however, could be a serious problem for tests in which one filtering direction is discarded; in this case, the LES model would vanish although the other two directions are poorly resolved. To avoid this difficulty, one should instead use the anisotropic version of the RLES model (12), in which δ_x,

TABLE I. Parameters for the numerical simulations.

Nominal Re_τ	$L_x\times L_y\times L_z$	$N_x\times N_y\times N_z$
180	$4\pi\times2\times4/3\pi$	$36\times37\times36$
395	$2\pi\times2\times\pi$	$72\times55\times54$

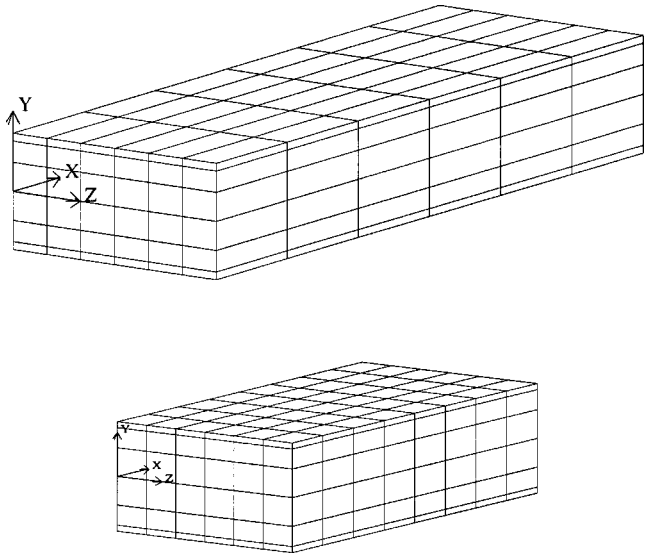

FIG. 3. Spectral element meshes: $\mathrm{Re}_\tau=180$ (top), and $\mathrm{Re}_\tau=395$ (bottom).

δ_y, and δ_z are all different. The derivation of this anisotropic form of the RLES model is straightforward and the resulting model remains easy to implement.

We used as a first step the RLES model (12) with the inverse operator equipped with Neumann boundary conditions.

The numerical simulations were performed by using a spectral element code based on the $\mathbb{P}_N-\mathbb{P}_{N-2}$ velocity and pressure spaces introduced by Maday and Patera.[43] The domain is decomposed into spectral elements, as shown in Fig. 3. Mesh spacing in the wall-normal direction (y) was chosen to be roughly equivalent to a Chebyshev distribution having the same number of points. The velocity is continuous across element interfaces and is represented by Nth-order tensor-product Lagrange polynomials based on the GLL points. The pressure is discontinuous and is represented by tensor-product polynomials of degree $N-2$. Time stepping is based on an operator splitting of the discrete system, which leads to separate convective, viscous, and pressure subproblems without the need for *ad hoc* pressure boundary conditions. A filter, which removes 2%–5% of the highest velocity mode, is used to stabilize the Galerkin formulation;[44] the filter does not compromise the spectral accuracy. Details of the discretization and solution algorithm are given in Refs. 45, 46.

The initial conditions for the $\mathrm{Re}_\tau=180$ simulations were obtained by superimposing a 2D Tollmien–Schlichting (TS) mode of 2% amplitude and a 3D TS mode of 1% amplitude on a parabolic mean flow (Poiseuille flow) and integrating the flow for a long time (approximately $200\,\mathrm{H}/u_\tau$) on a finer mesh ($72\times73\times72$ mesh points). The final field file was further integrated on the actual coarse LES mesh ($36\times37\times36$ mesh points) for approximately $50\,\mathrm{H}/u_\tau$ to obtain the initial condition for *all* three $\mathrm{Re}_\tau=180$ simulations.

The initial condition for the $\mathrm{Re}_\tau=395$ case was obtained in a similar manner: We started with a field file corresponding to a $\mathrm{Re}_\tau=180$ simulation, and we integrated it on a finer mesh ($96\times73\times72$ mesh points) for a long time (approximately $50\,\mathrm{H}/u_\tau$). Then, we integrated the resulting flow on the actual coarser LES mesh ($72\times55\times54$ mesh points) for another $40\,\mathrm{H}/u_\tau$, and the final field file was used as initial condition for *all* three simulations.

For each of the three simulations and for both $\mathrm{Re}_\tau=180$ and $\mathrm{Re}_\tau=395$, the flow was integrated further in time until the statistically steady state was reached (for approximately $15\,\mathrm{H}/u_\tau$). The statistically steady state was identified by a linear total shear stress profile. Figures 4 and 5 present results for ''coarse DNS'' (without any LES model) for $\mathrm{Re}_\tau=180$ and $\mathrm{Re}_\tau=395$, respectively. The total shear stress for the $\mathrm{Re}_\tau=395$ case tends to overshoot (undershoot) the correct values at the wall (-1 and 1, respectively). At the wall, however, the correct values are attained. One possible reason for this behavior is the fact that we impose a constant mass flux through the channel (instead of a constant pressure gradient) and to the inadequate resolution near the wall (the

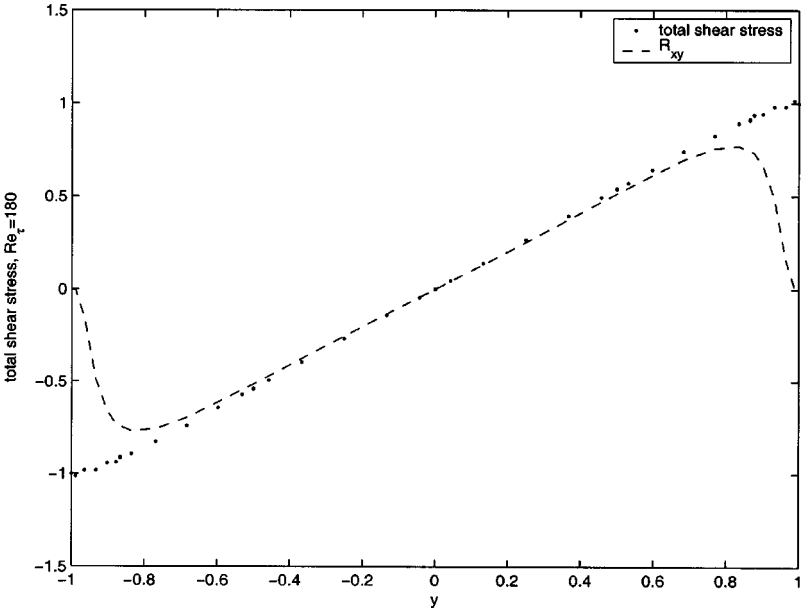

FIG. 4. $\mathrm{Re}_\tau=180$, linear total shear stress profile, an indication that the statistically steady state was reached.

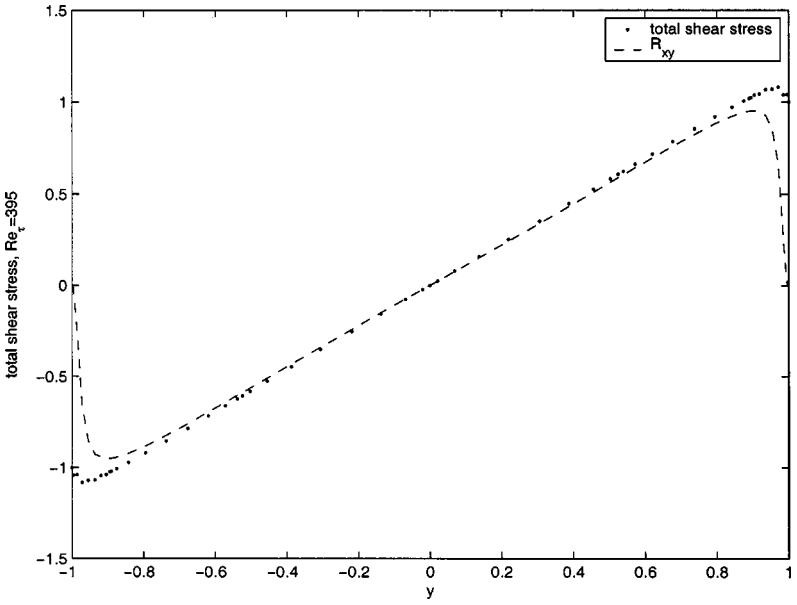

FIG. 5. $Re_\tau = 395$, linear total shear stress profile, an indication that the statistically steady state was reached.

first mesh point away from the wall is at $y^+ = 1.753\,368\,616$. This issue, which is part of the very complex interplay between the numerical method and the LES model employed, appears as an interesting avenue for further investigation.

The statistics were then collected over another $5\,H/u_\tau$ and contained samples taken after each time step ($\Delta t = 0.0002$ for $Re_\tau = 180$ and $\Delta t = 0.000\,25$ for $Re_\tau = 395$). We also averaged over the two halves of the channel.

Note that in our simulations the bulk velocity U_m was fixed to match the corresponding one in Ref. 42 (see Table II), and the friction velocity u_τ was a result of the simulations. Table II presents the *actual* values of Re_τ corresponding to the friction velocity u_τ computed for all four numerical tests and two nominal Reynolds numbers. We note that the friction velocity u_τ is within 1%–2% of the nominal value, and, as a result, so is the actual Re_τ.

In our numerical experiments, we considered, as a first step, homogeneous boundary conditions for all LES models tested.

The numerical results include plots of the following time- and plane-averaged (denoted by $\langle\cdot\rangle$) quantities normalized by the *computed* u_τ: the mean streamwise velocity, the *x, y* component of the Reynolds stress, and the rms values of the streamwise, wall-normal, and spanwise velocity fluctuations. We computed these statistics following the approach in Ref. 47, where it was proved that the best way to reconstruct the Reynolds stresses from LES is

$$R_{ij}^{\mathrm{DNS}} \approx R_{ij}^{\mathrm{LES}} + \langle \overline{A}_{ij}^{M} \rangle, \tag{13}$$

where $R_{ij}^{\mathrm{DNS}} \equiv \langle u_i u_j \rangle - \langle u_i \rangle \langle u_j \rangle$ are the Reynolds stresses from the fine DNS in Ref. 42, $R_{ij}^{\mathrm{LES}} \equiv \langle \overline{u_i} \overline{u_j} \rangle - \langle \overline{u_i} \rangle \langle \overline{u_j} \rangle$ are the Reynolds stresses corresponding to the dynamics of the LES field, and $\langle \overline{A}_{ij}^{M} \rangle$ are the averaged values of the modeled subgrid-scale stresses $\langle \tau_{ij} \rangle = \langle \overline{u_i u_j} - \overline{u_i} \overline{u_j} \rangle$.

As pointed out in Ref. 47, the Reynolds stresses from an LES can only be compared with those from a DNS by also taking into account the significant contribution from the averaged subgrid-scale stresses. Since we include results for the Smagorinsky model with Van Driest damping, we need to be careful with the reconstruction of the diagonal Reynolds stresses (the rms turbulence intensities). Specifically, for this eddy-viscosity model, only the *anisotropic* part of R_{ij}^{DNS} can be reconstructed (and thus compared with DNS)

$$R_{ii}^{*\mathrm{DNS}} \approx R_{ii}^{*\mathrm{LES}} + \langle \overline{A}_{ii}^{*M} \rangle, \tag{14}$$

where

$$R_{ii}^{*\mathrm{DNS}} \equiv \langle u_i' u_i' \rangle - \frac{1}{3} \sum_{k=1}^{3} \langle u_k' u_k' \rangle = R_{ii}^{\mathrm{DNS}} - \frac{1}{3} \sum_{k=1}^{3} R_{kk}^{\mathrm{DNS}},$$

TABLE II. Computed u_τ and Re_τ.

Fixed U_m	Nominal Re_τ	Case	Computed u_τ	Computed Re_τ
15.63	180	RLES	0.987 944 8	177.835 2
		Gradient	0.989 011 8	178.022 2
		Smagorinsky with Van Driest damping	0.991 714 4	178.512 0
17.54	395	RLES	1.001 025 319	395.407 196 0
		Gradient	1.005 021 334	396.985 992 4
		Smagorinsky with Van Driest damping	0.997 417 688 4	393.971 893 3

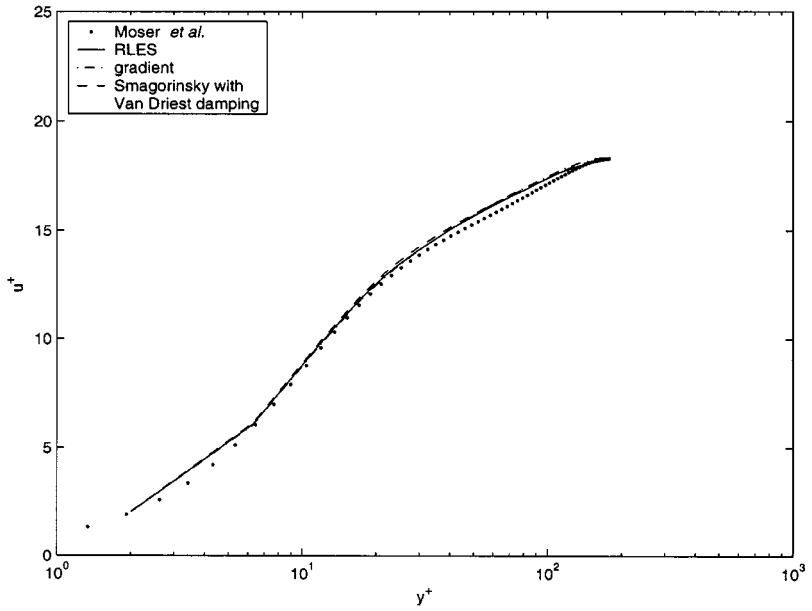

FIG. 6. Mean streamwise velocity, $\mathrm{Re}_\tau=180$. We compared the RLES model (12), the gradient model (9), and the Smagorinsky model with Van Driest damping with the fine DNS of Moser, Kim, and Mansour (Ref. 42).

$$u_i' \equiv u_i - \langle u_i \rangle,$$

$$R_{ii}^{*\mathrm{LES}} \equiv R_{ii}^{\mathrm{LES}} - \frac{1}{3}\sum_{k=1}^{3} R_{kk}^{\mathrm{LES}},$$

$$\overline{A}_{ii}^{*} \equiv \overline{A}_{ii} - \frac{1}{3}\sum_{k=1}^{3} \overline{A}_{kk},$$

and $\overline{A}_{ii}^{*M}$ is modeling $\overline{A}_{ii}^{*}$.

The reconstruction of the off-diagonal stresses R_{xy} is straightforward

$$R_{xy}^{\mathrm{DNS}} \approx R_{xy}^{\mathrm{LES}} + \langle \overline{A}_{xy}^{*M} \rangle, \tag{15}$$

since $\langle \overline{A}_{xy}^{*M} \rangle = \langle \overline{A}_{xy}^{M} \rangle$.

In computing R_{xy}, u_{rms}^{*}, v_{rms}^{*}, and w_{rms}^{*}, for the three LES models, we used formulas (14) and (15)

$$\begin{aligned} u_{\mathrm{rms}}^{*} &= (|R_{11}^{*\mathrm{LES}} + \langle \overline{A}_{11}^{*M} \rangle|)^{1/2}, \\ v_{\mathrm{rms}}^{*} &= (|R_{22}^{*\mathrm{LES}} + \langle \overline{A}_{22}^{*M} \rangle|)^{1/2}, \\ w_{\mathrm{rms}}^{*} &= (|R_{33}^{*\mathrm{LES}} + \langle \overline{A}_{33}^{*M} \rangle|)^{1/2}. \end{aligned} \tag{16}$$

These results were then compared with the corresponding ones in Ref. 42.

IV. *A POSTERIORI* TESTS FOR $\mathrm{Re}_\tau=180$

We ran *a posteriori* tests for the RLES model (12), the gradient model (9), and the Smagorinsky model with Van Driest damping. We compared the corresponding results with the fine DNS simulation of Moser, Kim, and Mansour.[42]

Figure 6 shows the normalized mean streamwise velocity u^+, where a "+" superscript denotes the variable in wall

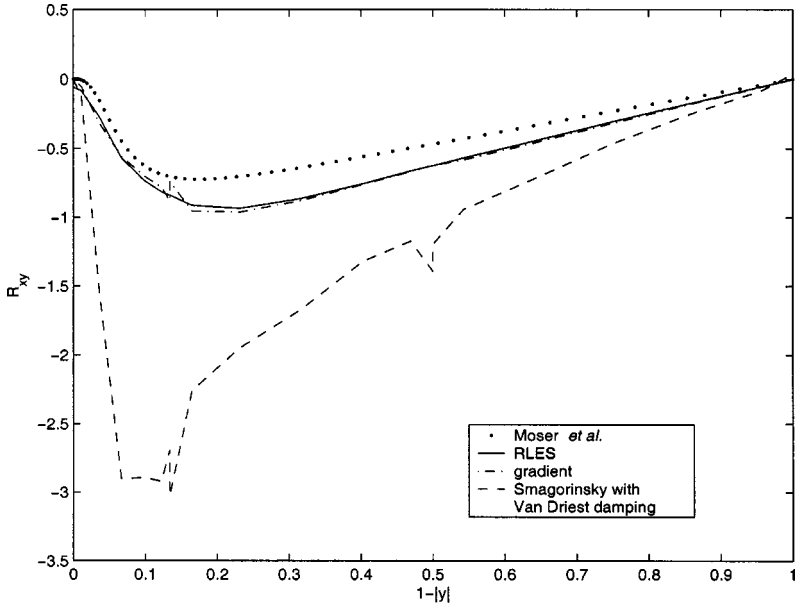

FIG. 7. The x, y component of the Reynolds stress, $\mathrm{Re}_\tau=180$. We compared the RLES model (12), the gradient model (9), and the Smagorinsky model with Van Driest damping with the fine DNS of Moser, Kim, and Mansour (Ref. 42).

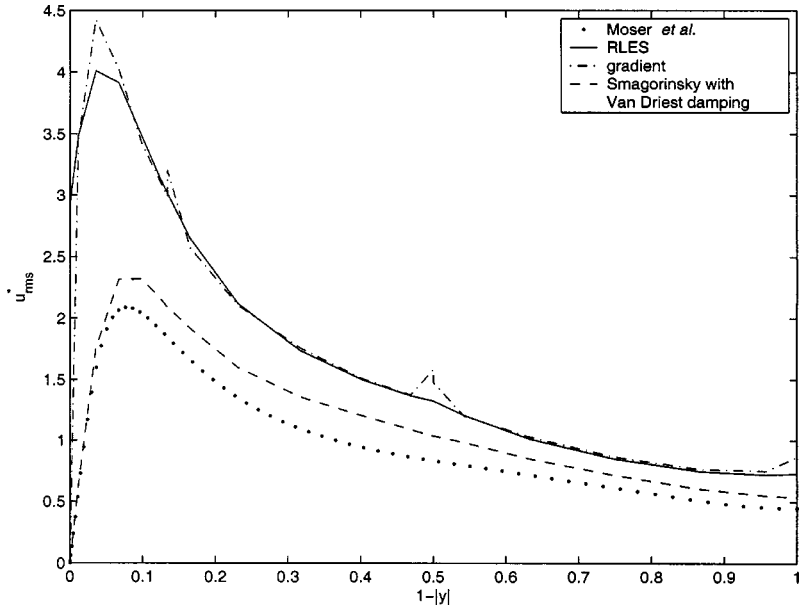

FIG. 8. rms values of streamwise velocity fluctuations, $\mathrm{Re}_\tau = 180$. We compared the RLES model (12), the gradient model (9), and the Smagorinsky model with Van Driest damping with the fine DNS of Moser, Kim, and Mansour (Ref. 42).

units; note the almost perfect overlapping of the results corresponding to the models tested. We interpret this behavior as a measure of our success in enforcing a constant mass flux through the channel. Since we have only two mesh points with $y^+ \leqslant 10$ away from the wall, the plotting by linear interpolation between these two points produces inadequate results. The mean streamwise velocity u^+ at these points is, however, very close to that in the fine DNS.

Figure 7 presents the normalized x, y component of the Reynolds stress, R_{xy}, computed by using (15). Note that R_{xy} includes contributions from the subgrid-scale stresses, which, in turn, include terms containing the gradient of the computed velocity. Since this gradient is not continuous across the spectral elements, we obtain the spikes in the gradient (9) and Smagorinsky with Van Driest damping models. The inverse operator in the RLES model (12) has a smoothing effect on the subgrid-scale stress tensor and attenuates these spikes. This behavior is apparent in all the other plots for the Reynolds stresses. The R_{xy} for the RLES model (RLES) is better than that corresponding to the gradient model (9) (there are no spikes), with the exception of the near-wall region; here, the inverse (smoothing) operator equipped with Neumann boundary conditions introduces a nonzero R_{xy} for the RLES model (12). Nevertheless, both the RLES (12) and the gradient (9) model yield much better results for R_{xy} than the Smagorinsky model with Van Driest damping; the latter performs poorly.

The situation is completely different for the rms turbulence intensities in Figs. 8–10: Here, the Smagorinsky model with Van Driest damping performs significantly better than both the RLES (12) and the gradient (9) models. As for the R_{xy}, the inverse operator in the RLES model has a smoothing effect and attenuates the spikes in the diagonal Reynolds stresses of the gradient model (9), yielding improved results,

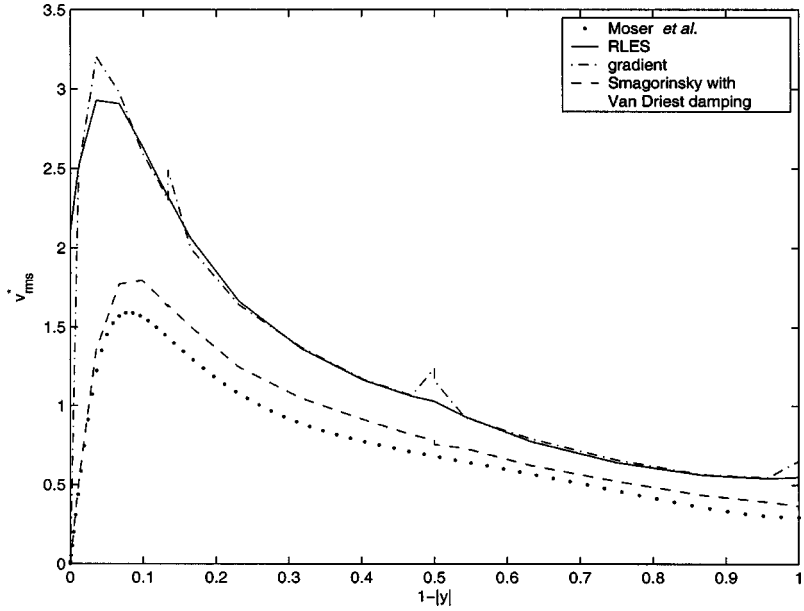

FIG. 9. rms values of wall-normal velocity fluctuations, $\mathrm{Re}_\tau = 180$. We compared the RLES model (12), the gradient model (9), and the Smagorinsky model with Van Driest damping with the fine DNS of Moser, Kim, and Mansour (Ref. 42).

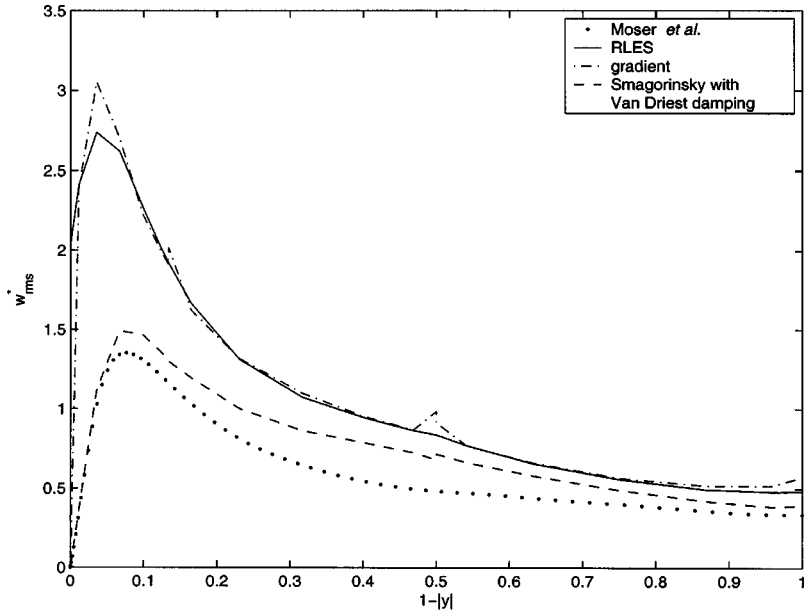

FIG. 10. rms values of spanwise velocity fluctuations, $\mathrm{Re}_\tau=180$. We compared the RLES model (12), the gradient model (9), and the Smagorinsky model with Van Driest damping with the fine DNS of Moser, Kim, and Mansour (Ref. 42).

with the exception of the near-wall region where it introduces a nonzero diagonal Reynolds stress. We also note that the first spike in the rms turbulence intensities for gradient model (9) away from the wall is *not* at the spectral element interface. Nevertheless, the smoothing operator in the RLES model (12) attenuates it significantly.

The inverse operator is also responsible for the much increased numerical stability of the RLES model (12) over the gradient model (9): In order to prevent the numerical simulations with the gradient model from blowing up, we had to use a very small time step; the simulations with the RLES model (12) ran with much larger time steps. (To collect statistics, however, we ran the two LES models with the same time step.)

V. *A POSTERIORI* TESTS FOR $\mathrm{Re}_\tau=395$

We ran simulations with all three LES models for $\mathrm{Re}_\tau=395$, and we compared our results with the fine DNS in Ref. 42. Again, as in the $\mathrm{Re}_\tau=180$ case, the normalized mean streamwise velocity profiles in Fig. 11 are practically identical; this time, however, they do not overlap onto that corresponding to the fine DNS. Nevertheless, the mean flows are the same, and this is supported by the fact that the models underpredict the correct value near the wall but overpredict it away from the wall. The inadequate behavior near the wall is due to the plotting, as in the $\mathrm{Re}_\tau=180$ case (we used linear interpolation for the two mesh points with $y^+\leqslant 10$ away from the wall). In fact, u^+ at these two mesh points com-

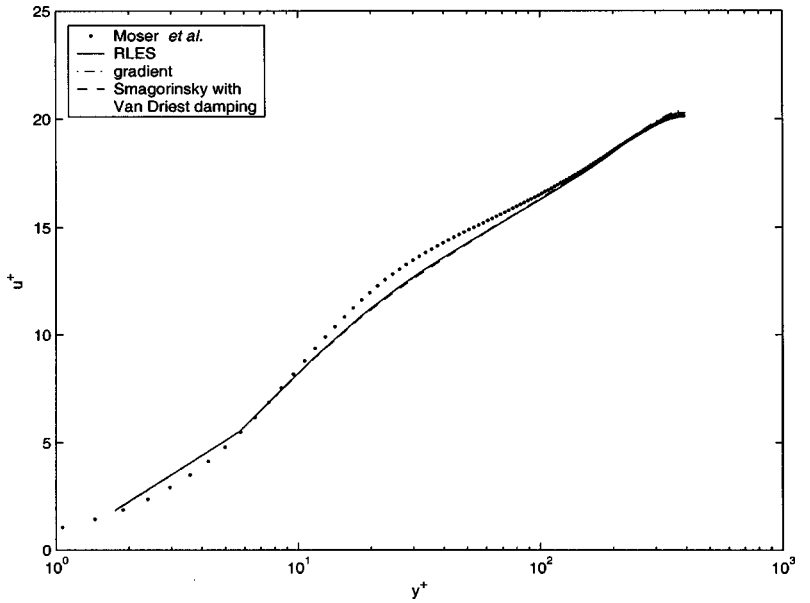

FIG. 11. Mean streamwise velocity, $\mathrm{Re}_\tau=395$. We compared the RLES model (12), the gradient model (9), and the Smagorinsky model with Van Driest damping with the fine DNS of Moser, Kim, and Mansour (Ref. 42).

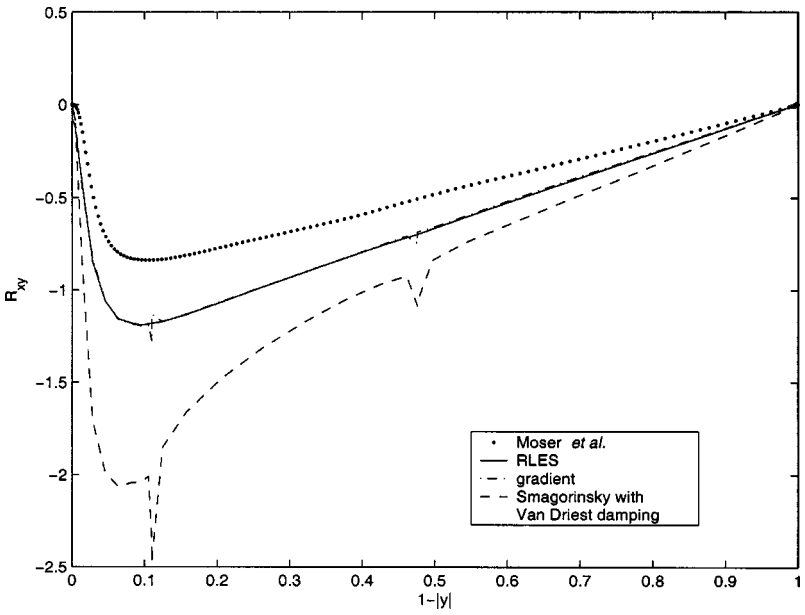

FIG. 12. The x, y component of the Reynolds stress, $\mathrm{Re}_\tau=395$. We compared the RLES model (12), the gradient model (9), and the Smagorinsky model with Van Driest damping with the fine DNS of Moser, Kim, and Mansour (Ref. 42).

pares very well with the fine DNS results in Ref. 42. In the buffer and log layers the three LES models deviate from the correct DNS results, but they perform well at the center of the channel.

The results for the normalized Reynolds stresses in Figs. 12–15 parallel the corresponding ones for the $\mathrm{Re}_\tau=180$ case: The RLES model (12) performs better than the gradient model (9) (the smoothing operator eliminates the spikes), with the exception of the near-wall region, where the smoothing operator introduces a nonzero value.

Both the RLES (12) and the gradient (9) models yield much better results for the off-diagonal Reynolds stress tensor R_{xy} than the Smagorinsky model with Van Driest damping (Fig. 12).

However, the Smagorinsky model with Van Driest damping performs much better than both the RLES (12) and the gradient (9) models in predicting the rms turbulence intensities (Figs. 13–15), with the exception of w^*_{rms} in Fig. 15, where the improvement is not that dramatic.

Again, as in the $\mathrm{Re}_\tau=180$ case, the RLES model (12) is much more stable numerically than the gradient model.

VI. CONCLUSIONS

We have used a spectral element code to test the RLES model (12) in the numerical simulation of incompressible channel flows at $\mathrm{Re}_\tau=180$ and $\mathrm{Re}_\tau=395$. This approximate deconvolution model is based on a rational (Padé) approximation to the Fourier transform of the Gaussian filter and is proposed as an alternative to the gradient model (9). We compared the RLES model (12) with the gradient model (9), and the Smagorinsky model with Van Driest damping. The

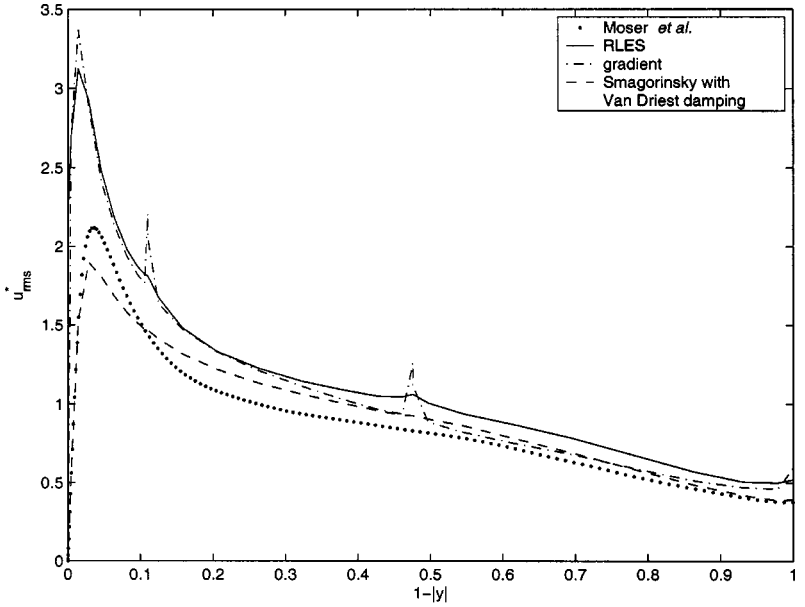

FIG. 13. rms values of streamwise velocity fluctuations, $\mathrm{Re}_\tau=395$. We compared the RLES model (12), the gradient model (9), and the Smagorinsky model with Van Driest damping with the fine DNS of Moser, Kim, and Mansour (Ref. 42).

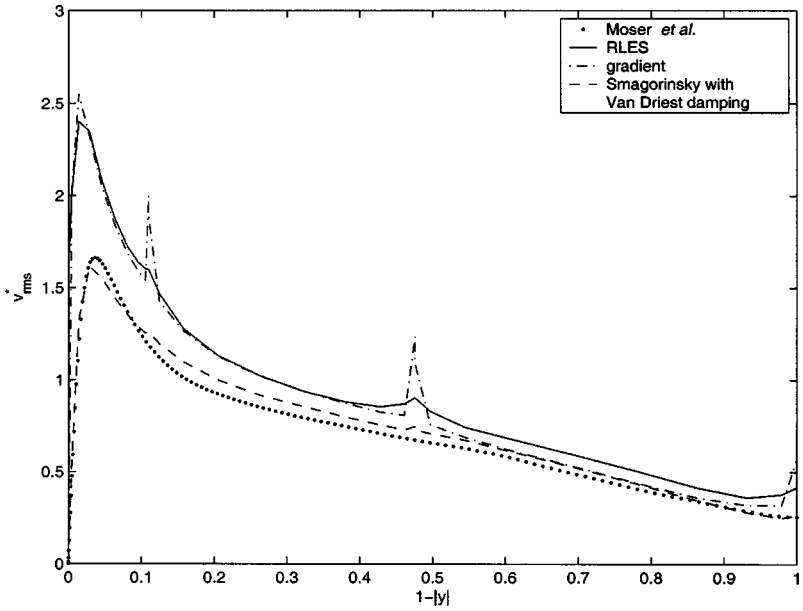

FIG. 14. rms values of wall-normal velocity fluctuations, $Re_\tau=395$. We compared the RLES model (12), the gradient model (9), and the Smagorinsky model with Van Driest damping with the fine DNS of Moser, Kim, and Mansour (Ref. 42).

corresponding results were benchmarked against the fine DNS calculation of Moser, Kim, and Mansour.[42]

The RLES model (12) yielded better results than the gradient model (9) for both $Re_\tau=180$ and $Re_\tau=395$, and for all Reynolds stresses. This was due to the inverse operator in the RLES model, which had a smoothing effect over the modeled subgrid-scale stress tensor and eliminated (or attenuated) the spikes in the gradient model. The inverse operator equipped with Neumann boundary conditions, however, introduced nonzero Reynolds stresses in the near-wall region.

But, the most significant improvement of the RLES model over the gradient model is the much increased numerical stability, which is also due to the smoothing effect of the inverse operator.

The Smagorinsky model with Van Driest damping performed worse than both the RLES and the gradient models in predicting the off-diagonal Reynolds stresses, but predicted very accurately the rms turbulent fluctuations.

We believe that these results for the RLES model are encouraging. They also support our initial thoughts: The RLES model is an improvement over the gradient model as a *subfilter-scale* model. The RLES model is also more stable numerically because of the additional smoothing operator, and this feature is manifest for both low ($Re_\tau=180$) and moderate ($Re_\tau=395$) Reynolds number flows.

However, the RLES model accounts just for the subfilter-scale part of the stress reconstruction. The information lost at the subgrid-scale level must be accounted for in a different way, as advocated by Carati *et al.*[24] This was illustrated by the dramatic improvement for the diagonal Reynolds stresses, for both $Re_\tau=180$ and $Re_\tau=395$, yielded by the Smagorinsky model with Van Driest damping, a classical eddy-viscosity model.

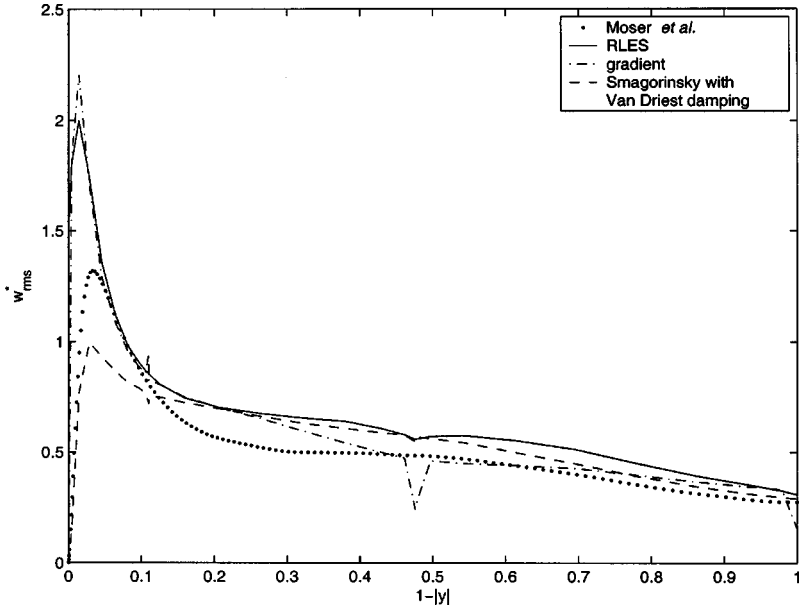

FIG. 15. rms values of spanwise velocity fluctuations, $Re_\tau=395$. We compared the RLES model (12), the gradient model (9), and the Smagorinsky model with Van Driest damping with the fine DNS of Moser, Kim, and Mansour (Ref. 42).

We believe that the RLES model (12), although an improvement over the gradient model (9), might not be competitive yet in challenging wall-bounded turbulent flow simulations; it should probably be supplemented by an eddy-viscosity mechanism (a mixed model). We plan to investigate this mixed model in more challenging simulations and compare our results with state-of-the-art LES models such as the dynamic Smagorinsky model[7] and the variational multiscale method of Hughes *et al.*[48–50]

We also plan to investigate the RLES model with the inverse operator equipped with homogeneous boundary conditions instead of Neumann boundary conditions as in the present simulations. This new boundary oconditions could yield a better behavior near the wall for the RLES model (12).

Other research directions include the study of improved boundary conditions, the commutation error,[51,52] and the relationship between the filter radius and the mesh size in a spectral element discretization.

ACKNOWLEDGMENTS

This work was supported in part by the Mathematical, Information, and Computational Sciences Division subprogram of the Office of Advanced Scientific Computing Research, U.S. Department of Energy, under Contract No. W-31-109-Eng-38, by the U.S. Department of Energy, Office of Advanced Scientific Computing, SciDAC program ''The Terascale Simulation Tools and Techniques (TSTT) Center,'' and by NSF Grant No. DMS-0209309. The computations were carried out on the NERSC's IBM-SP machine. We thank the two reviewers and Professor D. Carati, Professor A. Domaradzki, Professor R. Moser, Professor O. Vasilyev, and A. Das for helpful communications that improved this paper.

[1] C. Meneveau and J. Katz, ''Scale invariance and turbulence models for large-eddy simulation,'' Annu. Rev. Fluid Mech. **32**, 1 (2000).
[2] M. Lesieur and O. Métais, ''New trends in large-eddy simulations of turbulence,'' Annu. Rev. Fluid Mech. **28**, 45 (1996).
[3] P. Sagaut, *Large Eddy Simulation for Incompressible Flows* (Springer, Berlin, 2001).
[4] J. Smagorinsky, ''General circulation experiments with the primitive equation. I. The basic experiment,'' Mon. Weather Rev. **91**, 99 (1963).
[5] R. A. Clark, J. H. Ferziger, and W. C. Reynolds, ''Evaluation of subgrid scale models using an accurately simulated turbulent flow,'' J. Fluid Mech. **91**, 1 (1979).
[6] J. Bardina, J. H. Ferziger, and W. C. Reynolds, ''Improved turbulence models based on large eddy simulation of homogeneous, incompressible, turbulent flows,'' Technical Report No. TF-19, Department of Mechanical Engineering, Stanford University, Stanford, CA, 1983.
[7] M. Germano, U. Piomelli, P. Moin, and W. Cabot, ''A dynamic subgrid-scale eddy viscosity model,'' Phys. Fluids A **3**, 1760 (1991).
[8] U. Piomelli, ''High Reynolds number calculations using the dynamic subgrid-scale stress model,'' Phys. Fluids A **5**, 1484 (1993).
[9] K. Horiuti, ''A new dynamic two-paramater mixed model for large-eddy simulation,'' Phys. Fluids **9**, 3443 (1997).
[10] F. Sarghini, U. Piomelli, and E. Balaras, ''Scale-similar models for large-eddy simulations,'' Phys. Fluids **11**, 1596 (1999).
[11] K. B. Shah and J. Ferziger, ''A new non-eddy viscosity subgrid-scale model and its application to turbulent flow,'' in *CTR Annual Research Briefs 1995* (Center for Turbulence Research, Stanford University and NASA Ames Research Center, Stanford, CA, 1995).
[12] B. J. Geurts, ''Inverse modeling for large-eddy simulation,'' Phys. Fluids **9**, 3585 (1997).
[13] G. J. M. Kuerten, B. J. Geurts, A. W. Vreman, and M. Germano, ''Dynamic inverse-modeling and its testing in large-eddy simulation of the mixing layer,'' Phys. Fluids **11**, 3778 (1999).
[14] J. A. Domaradzki and E. M. Saiki, ''A subgrid-scale model based on the estimation of unresolved scales of turbulence,'' Phys. Fluids **9**, 2148 (1997).
[15] J. A. Domaradzki and K.-C. Loh, ''The subgrid-scale estimation model in physical space estimation,'' Phys. Fluids **11**, 2330 (1999).
[16] K.-C. Loh and J. A. Domaradzki, ''The subgrid-scale estimation model on nonuniform grids,'' Phys. Fluids **11**, 3786 (1999).
[17] S. Stolz and N. A. Adams, ''An approximate deconvolution procedure for large-eddy simulation,'' Phys. Fluids **11**, 1699 (1999).
[18] S. Stolz, N. A. Adams, and L. Kleiser, ''An approximate deconvolution model for large-eddy simulation with application to incompressible wall-bounded flows,'' Phys. Fluids **13**, 997 (2001).
[19] S. Stolz, N. A. Adams, and L. Kleiser, ''The approximate deconvolution model for large-eddy simulations of compressible flows and its application to shock-turbulent-boundary-layer interaction,'' Phys. Fluids **13**, 2985 (2001).
[20] A. Leonard, ''Energy cascade in large eddy simulations of turbulent fluid flows,'' Adv. Geophys. **18A**, 237 (1974).
[21] S. Liu, C. Meneveau, and J. Katz, ''On the properties of similarity subgrid-scale models as deduced from measurements in a turbulent jet,'' J. Fluid Mech. **275**, 83 (1994).
[22] V. Borue and S. A. Orszag, ''Local energy flux and subgrid-scale statistics in three-dimensional turbulence,'' J. Fluid Mech. **366**, 1 (1998).
[23] G. S. Winckelmans, A. A. Wray, O. V. Vasilyev, and H. Jeanmart, ''Explicit-filtering large-eddy simulations using the tensor-diffusivity model supplemented by a dynamic Smagorinsky term,'' Phys. Fluids **13**, 1385 (2001).
[24] D. Carati, G. S. Winckelmans, and H. Jeanmart, ''On the modeling of the subgrid-scale and filtered-scale stress tensors in large-eddy simulation,'' J. Fluid Mech. **441**, 119 (2001).
[25] B. Vreman, ''Direct and large-eddy simulation of the compressible turbulent mixing layer,'' Ph.D. thesis, University of Twente, 1995.
[26] G.-H. Cottet and A. A. Wray, ''Anisotropic grid-based formulas for subgrid-scale models,'' in *Annual Research Briefs* (Center for Turbulence Research, Stanford University and NASA Ames, Stanford, CA, 1997), pp. 113–122.
[27] G.-H. Cottet and O. V. Vasilyev, ''Comparison of dynamic Smagorinsky and anisotropic subgrid-scale models,'' in *Proceedings of the Summer Program* (Center for Turbulence Research, Stanford University and NASA Ames, Stanford, CA, 1998), pp. 367–388.
[28] B. Vreman, B. Geurts, and H. Kuerten, ''Large-eddy simulation of the temporal mixing layer,'' J. Fluid Mech. **339**, 357 (1997).
[29] G. P. Galdi and W. J. Layton, ''Approximating the larger eddies in fluid motion. II. A model for space filtered flow,'' Math. Models Methods Appl. Sci. **10**, 343 (2000).
[30] B. Vreman, B. Geurts, and H. Kuerten, ''Large-eddy simulation of the temporal mixing layer using the mixed Clark model,'' Theor. Comput. Fluid Dyn. **8**, 309 (1996).
[31] A. A. Aldama, *Filtering Techniques for Turbulent Flow Simulation*, Lecture Notes in Engineering 56, edited by C. A. Brebbia and S. A. Orszag (Springer, Berlin, 1990).
[32] F. V. Katopodes, R. L. Street, and J. H. Ferziger, ''Subfilter-scale scalar transport for large-eddy simulation,'' in *14th Symposium on Boundary Layers and Turbulence* (American Meteorological Society, Aspen, CO, 2000), pp. 472–475.
[33] M. Germano, ''Differential filters for the large eddy numerical simulation of turbulent flows,'' Phys. Fluids **29**, 1755 (1986).
[34] J. S. Mullen and P. F. Fischer, ''Filtering techniques for complex geometry fluid flows,'' Commun. Numer. Methods Eng. **15**, 9 (1999).
[35] J. A. Domaradzki and D. D. Holm, ''Navier–Stokes-alpha model: LES equations with nonlinear dispersion,'' in Modern Simulation Strategies for Turbulent Flow, edited by B. J. Geurts (ERCOFTAC Bulletin **48**, 2001).
[36] L. C. Berselli, G. P. Galdi, T. Iliescu, and W. J. Layton, ''Mathematical analysis for the rational large eddy simulation model,'' Math. Models Methods Appl. Sci. **12**, 1131 (2002).
[37] T. Iliescu, V. John, and W. J. Layton, ''Convergence of finite element approximation of large eddy motion,'' Num. Methods Partial Differ. Equ. **18**, 689 (2002).
[38] T. Iliescu, V. John, W. J. Layton, G. Matthies, and L. Tobiska, ''A numerical study of a class of LES models,'' Int. J. Comput. Fluid Dyn. **17**, 75 (2003).

[39]P. Fischer and T. Iliescu, "A 3D channel flow simulation at $Re_\tau=180$ using a rational LES model," in *Proceedings of Third AFOSR International Conference on DNS/LES*, edited by C. Liu, L. Sakell, and T. Beutner (Greyden, Columbus, 2001), pp. 283–290.
[40]P. Moin and J. Kim, "Numerical investigation of turbulent channel flow," J. Fluid Mech. **118**, 341 (1982).
[41]J. Kim, P. Moin, and R. Moser, "Turbulence statistics in fully developed channel flow at low Reynolds number," J. Fluid Mech. **177**, 133 (1987).
[42]D. R. Moser, J. Kim, and N. N. Mansour, "Direct numerical simulation of turbulent channel flow up to $Re_\tau=590$," Phys. Fluids **11**, 943 (1999).
[43]Y. Maday and A. T. Patera, "Spectral element methods for the Navier–Stokes equations," in *State of the Art Surveys in Computational Mechanics*, edited by A. K. Noor (ASME, New York, 1989), pp. 71–143.
[44]P. F. Fischer and J. S. Mullen, "Filter-based stabilization of spectral element methods," C. R. Acad. Sci., Ser. I: Math. **332**, 265 (2001).
[45]P. F. Fischer, "An overlapping Schwarz method for spectral element solution of the incompressible Navier–Stokes equations," J. Comput. Phys. **133**, 84 (1997).
[46]P. F. Fischer, N. I. Miller, and H. M. Tufo, "An overlapping Schwarz method for spectral element simulation of three-dimensional incompressible flows," in *Parallel Solution of Partial Differential Equations*, edited by P. Björstad and M. Luskin (Springer, Berlin, 2000), pp. 159–181.
[47]G. S. Winckelmans, H. Jeanmart, and D. Carati, "On the comparison of turbulence intensities from large-eddy simulation with those from experiment or direct numerical simulation," Phys. Fluids **14**, 1809 (2002).
[48]T. J. R. Hughes, L. Mazzei, and K. E. Jansen, "Large eddy simulation and the variational multiscale method," Comput. Vis. Sci. **3**, 47 (2000).
[49]T. J. R. Hughes, L. Mazzei, A. A. Oberai, and A. A. Wray, "The multiscale formulation of large eddy simulation: Decay of isotropic homogeneous turbulence," Phys. Fluids **13**, 505 (2001).
[50]T. J. R. Hughes, A. A. Oberai, and L. Mazzei, "Large eddy simulations of turbulent channel flows by the variational multiscale method," Phys. Fluids **13**, 1784 (2001).
[51]S. Ghosal and P. Moin, "The basic equations for the large-eddy simulation of turbulent flows in complex geometry," J. Comput. Phys. **118**, 24 (1995).
[52]S. Ghosal, "An analysis of numerical errors in large-eddy simulations of turbulence," J. Comput. Phys. **125**, 187 (1996).